



**HAL**  
open science

**Experimental and computational investigation of Z/E isomerism, X-ray crystal structure and molecular docking study of (2-(hydroxyimino)cyclohexyl)diphenylphosphine sulfide, a potential antibacterial agent**

Nejib Jebli, Youssef Arfaoui, Kristof van Hecke, Jean-François Cavalier, Soufiane Touil

► **To cite this version:**

Nejib Jebli, Youssef Arfaoui, Kristof van Hecke, Jean-François Cavalier, Soufiane Touil. Experimental and computational investigation of Z/E isomerism, X-ray crystal structure and molecular docking study of (2-(hydroxyimino)cyclohexyl)diphenylphosphine sulfide, a potential antibacterial agent. *Journal of Molecular Structure*, 2020, pp.129634. 10.1016/j.molstruc.2020.129634 . hal-03046712

**HAL Id: hal-03046712**

**<https://hal.science/hal-03046712>**

Submitted on 8 Dec 2020

**HAL** is a multi-disciplinary open access archive for the deposit and dissemination of scientific research documents, whether they are published or not. The documents may come from teaching and research institutions in France or abroad, or from public or private research centers.

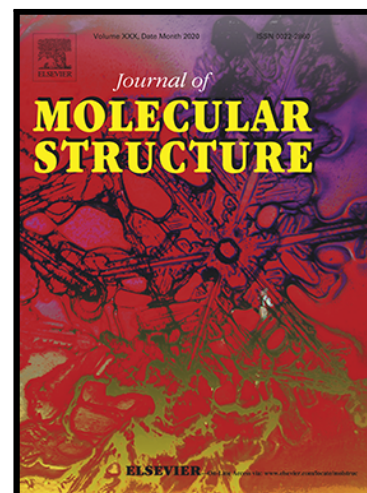
L'archive ouverte pluridisciplinaire **HAL**, est destinée au dépôt et à la diffusion de documents scientifiques de niveau recherche, publiés ou non, émanant des établissements d'enseignement et de recherche français ou étrangers, des laboratoires publics ou privés.

## Journal Pre-proof

Experimental and computational investigation of Z/E isomerism, X-ray crystal structure and molecular docking study of (2-(hydroxyimino)cyclohexyl)diphenylphosphine sulfide, a potential antibacterial agent

Nejib Jebli , Youssef Arfaoui , Kristof Van Hecke ,  
Jean-François Cavalier , Soufiane Touil

PII: S0022-2860(20)31947-5  
DOI: <https://doi.org/10.1016/j.molstruc.2020.129634>  
Reference: MOLSTR 129634



To appear in: *Journal of Molecular Structure*

Received date: 9 October 2020  
Revised date: 8 November 2020  
Accepted date: 10 November 2020

Please cite this article as: Nejib Jebli , Youssef Arfaoui , Kristof Van Hecke , Jean-François Cavalier , Soufiane Touil , Experimental and computational investigation of Z/E isomerism, X-ray crystal structure and molecular docking study of (2-(hydroxyimino)cyclohexyl)diphenylphosphine sulfide, a potential antibacterial agent, *Journal of Molecular Structure* (2020), doi: <https://doi.org/10.1016/j.molstruc.2020.129634>

This is a PDF file of an article that has undergone enhancements after acceptance, such as the addition of a cover page and metadata, and formatting for readability, but it is not yet the definitive version of record. This version will undergo additional copyediting, typesetting and review before it is published in its final form, but we are providing this version to give early visibility of the article. Please note that, during the production process, errors may be discovered which could affect the content, and all legal disclaimers that apply to the journal pertain.

© 2020 Published by Elsevier B.V.

**Highlights**

- The structure of a novel thiophosphoryl oxime was studied by FT-IR, NMR and XRD.
- The title compound equilibrates in solution to give a mixture of *E* and *Z* isomers.
- Nitrogen inversion is the most probable mechanism for *Z/E* isomerization.
- DFT calculations predicted better antibacterial activity for the *Z* isomer.
- Molecular docking in *EcFabH* enzyme showed high inhibitory effect for the *Z* isomer.

Journal Pre-proof

# Experimental and computational investigation of *Z/E* isomerism, X-ray crystal structure and molecular docking study of (2-(hydroxyimino)cyclohexyl)diphenylphosphine sulfide, a potential antibacterial agent

Nejib Jebli <sup>a</sup>, Youssef Arfaoui <sup>b</sup>, Kristof Van Hecke <sup>c</sup>, Jean-François Cavalier <sup>d</sup>, Soufiane Touil <sup>a</sup>

<sup>a</sup>Laboratory of Hetero-Organic Compounds and Nanostructured Materials (LR18ES11), University of Carthage, Faculty of Sciences of Bizerte, 7021 Jarzouna, Tunisia.

<sup>b</sup>University of Tunis El Manar, Faculty of Sciences of Tunis, Laboratory of Characterizations, Applications and Modeling of Materials, 2092 El Manar II, Tunis, Tunisia.

<sup>c</sup>XStruct, Department of Chemistry, Ghent University, Krijgslaan 281-S3, 9000 Ghent, Belgium.

<sup>d</sup>Aix-Marseille Univ, CNRS, LISM, Institut de Microbiologie de la Méditerranée (IMM FR3479), Marseille, France.

## ABSTRACT

(2-(hydroxyimino)cyclohexyl)diphenylphosphine sulfide [C<sub>18</sub>H<sub>20</sub>NOPS (**2**)] is a novel oxime derivative that has been identified, in a recent work from our group, as a potential antibacterial agent. Herein, we report the in-depth structural analysis of compound (**2**) by using various spectroscopic tools including FT-IR, NMR (<sup>1</sup>H, <sup>31</sup>P, <sup>13</sup>C), mass spectrometry and single crystal X-ray diffraction, which indicate that it is obtained as a mixture of *Z* and *E* isomers. The different mechanisms, inversion, rotation, or mixed inversion-rotation, by which could occur the *Z/E* isomerization, have been investigated computationally with DFT method. Total and frontier molecular orbitals energies for both isomers were derived in order to gain more insights into their relative stabilities and biological activities. *In silico* molecular docking studies in *E. coli* FabH enzyme active site were also performed to predict the possible interaction modes and binding energies for both *Z* and *E* isomers as compared with those of a reference FabH inhibitor.

**Keywords:** oximes; phosphine sulfides; *Z/E* isomerism; X-ray diffraction; DFT calculations; *in silico* molecular docking; FabH inhibitors; antibacterial activity.

## 1. Introduction

Oxime derivatives have aroused the continuing strong interest of researchers over the past few decades due to their great importance and wide-range applications as antimicrobial [1], antiparasitic [2], antiviral [3], antihistaminic [4], anticancer [5] and anti-HIV [6] agents. In addition, some oximes are also known for their applications as antidotes against poisoning by pesticides and chemical weapons [7].

On the other hand, organophosphorus derivatives are an important class of compounds in medicinal chemistry that possess interesting biological effects and differential binding affinities to diverse microbiological targets [8], and the introduction of a phosphoryl or thiophosphoryl group to the oxime unit could improve the biological activity of such compounds, in conformity with the active substructure combination principle [9]. This is confirmed by a number of papers showing that phosphines, as well as their phosphine oxide or phosphine sulfide derivatives, exhibit promising antimicrobial, anticancer or antiarthritic activities [10].

In the frame of our research program on the synthesis and evaluation of novel phosphorus-containing compounds with possible biological properties [11], we recently described an efficient approach to unprecedented  $\alpha$ -(diphenylphosphoryl)- and  $\alpha$ -(diphenylphosphorothioyl)cycloalkanone oximes, by using a two-step synthetic pathway from cyclic enamines, *via* the oximation of the  $\alpha$ -(diphenylphosphoryl)- and  $\alpha$ -(diphenylphosphorothioyl)cycloalkanones intermediates [12]. The obtained phosphorus-containing oximes have shown promising antibacterial activities, what prompted us for further investigations to gain a deeper understanding of their structural and biological properties.

To reach this goal, we select the  $\alpha$ -(diphenylphosphorothioyl)cycloalkanone oxime derivative (**2**) [(2-(hydroxyimino)cyclohexyl)diphenylphosphine sulfide, C<sub>18</sub>H<sub>20</sub>NOPS] which was obtained as a mixture of *Z* and *E* isomers in 42:58 ratio, and was found to display high antibacterial activities against Gram-positive (*i.e.*, *Staphylococcus aureus* and *Bacillus subtilis*) and Gram-negative (*i.e.*, *Escherichia coli* and *Salmonella typhimurium*) bacteria with minimal inhibitory concentrations, MIC, in the range 0.9-1.8  $\mu$ g/mL and minimal bactericidal concentrations, MBC, around 2.0  $\mu$ g/mL (see compound **2d** in reference [12]). Herein, we report the spectroscopic characterization and structural study by X-ray diffraction of this phosphorus-containing oxime (**2**). The mechanism of *Z/E* isomerization at the C=N double bond has been investigated computationally with DFT method. Molecular docking and DFT calculations were used to compare the antibacterial activities of the *Z* and *E* isomers.

## 2. Experimental

### 2.1. Chemical preparation of (2-(hydroxyimino)cyclohexyl)diphenylphosphine sulfide (**2**)

The studied compound C<sub>18</sub>H<sub>20</sub>NOPS (**2**) was prepared by using a two-step synthetic pathway from a cyclic enamine, *via* the oximation of 2-

(diphenylphosphorothioyl)cyclohexanone intermediate (**1**), according to the recently reported procedure developed by our group [12].

### 2.1.1. Synthetic protocol for 2-(diphenylphosphorothioyl)cyclohexanone intermediate (**1**)

To a well stirred solution of enamine [1-morpholinocyclohexene] [13] (1 mmol) and triethylamine (1.1 mmol) in dry acetonitrile (15 mL), maintained under an inert atmosphere ( $N_2$ ) and cooled at 0 °C, *P*-chlorodiphenylphosphine (1 mmol) in dry acetonitrile (3 mL) was added dropwise within 15 min. The resulting solution was warmed up to room temperature and stirred for 2 h. Ground sulfur (1 mmol) was then added and the reaction mixture was stirred at room temperature for 2 h until complete dissolution of the sulfur. 2N aqueous HCl solution (30 mL) was then added dropwise at 0 °C and stirring was continued at room temperature for 12 h. The mixture was then extracted with  $CH_2Cl_2$  (3×10 mL). The organic phase was dried over  $MgSO_4$  and concentrated under vacuum. The residue obtained was chromatographed on a silica gel column using *n*-hexane/ethyl acetate (1:1, v/v) as eluent, to afford the pure product (**1**) as a white solid in 91% yield.

### 2.1.2. Synthetic protocol for (2-(hydroxyimino)cyclohexyl)diphenylphosphine sulfide (**2**)

A solution of 2-(diphenylphosphorothioyl)cyclohexanone (**1**) (0.01 mol) in dry ethanol (10 mL) was added dropwise with stirring at 25 °C to a mixture of hydroxylamine hydrochloride (0.01 mol), potassium hydroxide (0.01 mol) and dry ethanol (20 mL). The reaction mixture was then heated under reflux for 24 h. The progress of reaction was monitored by checking TLC at regular intervals. After cooling, the solvent was removed under reduced pressure. The residue obtained was diluted with  $CHCl_3$  (30 mL) and washed with water (2×20 mL). The organic phase was dried over  $Na_2SO_4$  and concentrated under vacuum. The residue obtained was chromatographed on a silica gel column using *n*-hexane/ethyl acetate (6:4, v/v) as eluent, to afford the pure product (**2**) as a yellow solid in 87% yield.

mp 49 °C; FT-IR ( $CHCl_3$ ):  $\nu_{P=S}$  698  $cm^{-1}$ ;  $\nu_{C=N}$  1638  $cm^{-1}$ ;  $\nu_{OH}$  3343  $cm^{-1}$ .  $^{31}P$  NMR ( $CDCl_3$ , 161.97 MHz):  $\delta$  (ppm) = 45.16 (s, 42 %, *Z*-stereoisomer), 45.44 (s, 58 %, *E*-stereoisomer).  $^1H$  NMR ( $CDCl_3$ , 400.13 MHz):  $\delta$  = 1.42-2.93 (m, 8 H, 4  $CH_2$ , *Z* & *E*-stereoisomers), 3.69-3.74 (m, 1H, CH-P, *E*-stereoisomer), 4.86-4.90 (m, 1H, CH-P, *Z*-stereoisomer), 7.29-8.18 (m, 10 H, Ar-H, *Z* & *E*-stereoisomers), 9.00 (br s, 1H, OH, *Z* & *E*-stereoisomers).  $^{13}C$  NMR ( $CDCl_3$ , 100.61 MHz):  $\delta$  = 21.8 (s,  $CH_2-CH_2-CH$ , *E*-stereoisomer), 23.1 (d,  $CH_2-CH_2-CH$ ,  $^3J_{CP}$  = 4.0 Hz, *Z*-stereoisomer), 24.1 (d,  $CH_2-CH_2-C=N$ ,  $^4J_{CP}$  = 1.0 Hz, *Z*-stereoisomer), 25.1 (s,  $CH_2-$

CH<sub>2</sub>-C=N, *E*-stereoisomer), 26.8 (s, CH<sub>2</sub>-CH, *Z*-stereoisomer), 27.4 (s, CH<sub>2</sub>-CH, *E*-stereoisomer), 30.9 (s, CH<sub>2</sub>-C=N, *E*-stereoisomer), 31.3 (s, CH<sub>2</sub>-C=N, *Z*-stereoisomer), 34.8 (d, CH-P, <sup>1</sup>J<sub>CP</sub> = 39.2 Hz, *Z*-stereoisomer), 42.2 (d, CH-P, <sup>1</sup>J<sub>CP</sub> = 42.3 Hz, *E*-stereoisomer), 156.5 (d, C=N, <sup>2</sup>J<sub>CP</sub> = 4.0 Hz, *Z*-stereoisomer), 156.6 (d, C=N, <sup>2</sup>J<sub>CP</sub> = 4.0 Hz, *E*-stereoisomer), Ar-C: δ = 127.77, 127.86, 128.05, 128.17, 128.26, 128.35, 128.45, 128.58, 128.67, 128.70, 128.75, 128.79, 128.84, 128.89, 131.07, 131.10, 131.16, 131.18, 131.22, 131.26, 131.28, 131.30, 131.39, 131.42, 131.50, 131.59, 131.64, 131.66, 131.72, 131.74, 131.83, 131.88, 131.91, 131.95, 132.19, 132.28, 132.52, 132.55, 132.83. EI-HRMS: calculated for C<sub>18</sub>H<sub>20</sub>NOPS: 329.3978 (M<sup>+</sup>); found: 329.3979.

## 2.2. Investigation techniques

### 2.2.1. FT-IR, NMR and mass spectrometry

Compound (**2**) was characterized by FT-IR, NMR and mass spectrometry. The infrared spectrum was recorded in the 400–4000 cm<sup>-1</sup> range with a Nicolet IR200 FT-IR spectrometer using a CHCl<sub>3</sub> solution at ambient temperature. The number of scans was 32 and the resolution 4 cm<sup>-1</sup>. NMR spectra were recorded at 400 MHz (<sup>1</sup>H), 161 MHz (<sup>31</sup>P) and 100 MHz (<sup>13</sup>C APT) in CDCl<sub>3</sub>. Chemical shifts (δ) are reported in part per million (ppm) relative to the residual solvent peak. The coupling constants are reported in Hz. The multiplicities of signals are indicated by the following abbreviations: s: singlet; d: doublet; t: triplet; and m: multiplet. High-resolution-MS spectrum was performed on a JEOL JMSGC mateII mass spectrometer.

### 2.2.2. X-ray diffraction experiments

The X-ray intensity data of compound C<sub>18</sub>H<sub>20</sub>NOPS (**2**) was collected at 100 K, on a Rigaku Oxford Diffraction Supernova Dual Source (Cu at zero) diffractometer equipped with an Atlas CCD detector using ω scans and CuKα (λ = 1.54184 Å) radiation. The images were interpreted and integrated with the program CrysAlisPro (Rigaku Oxford Diffraction) [14]. Using Olex2 [15], the structure was solved by direct methods using the ShelXS [16] structure solution program and refined by full-matrix least-squares on F<sup>2</sup> using the ShelXL [17] program package. Non-hydrogen atoms were anisotropically refined and the hydrogen atoms in the riding mode and isotropic temperature factors fixed at 1.2 times U(eq) of the parent atoms (1.5 times for methyl groups). The drawings were made with Diamond [18] and

Mercury [19]. Crystal data and experimental parameters used for the intensity data collection are summarized in **Table 1**.

### 2.2.3. DFT calculations

All calculations were performed using Gaussian 09 program [20]. Electronic structures, optimized geometrical parameters and transition states were calculated by density functional theory (DFT) with B3LYP/6-311++G(d,p) basis set. The frontier molecular orbital surfaces are visualized by Gauss View Molecular Visualization program [21].

### 2.2.4. Molecular docking experiments

The Autodock Vina program [22] was used to generate the putative binding modes of both the *Z*-(**2**) and *E*-(**2**) isomers into the active site of the *E. coli*  $\beta$ -ketoacyl-acyl carrier protein synthase III (*EcFabH*) as previously reported [12, 23]. For the sake of comparison, the (*E*)-*N*-((3,4-dihydro-2*H*-benzo[*b*][1,4]dioxepin-7-yl)methylene)-hexadecan-1-amine (*i.e.*, **Cpd10**) which is an effective inhibitor of *EcFabH* [23c] was also docked in the enzyme active site. The PyMOL Molecular Graphics System (version 1.4, Schrödinger, LLC) was used as working environment with an in-house version of the AutoDock/Vina PyMOL plugin [24]. The X-ray crystallographic structure of *EcFabI* in complex with Malonyl-CoA (PDB entry code: 1HNJ; 1.46 Å resolution) [25] available at the Protein Data Bank was used as receptor. Docking runs were performed after removing the Malonyl-CoA ligand from the enzyme active site. The box size used for the receptor fit the whole active site cleft and allowed non-constructive binding positions. The three-dimensional structures of the aforementioned compounds were constructed using Chem 3D ultra 11.0 software [Chemical Structure Drawing Standard; Cambridge Soft corporation, USA (2007)], and their geometry was refined using the Avogadro open-source molecular builder and visualization tool (version 1.2.0. <http://avogadro.cc/>).

The accuracy of the docking experiment was checked by submitting the 1-(5-(2-Fluoro-5-(hydroxymethyl)phenyl)pyridin-2-yl)piperidine-4-carboxylic acid inhibitor (*i.e.*, **Cpd23** – *EcFabH* IC<sub>50</sub> = 0.53 μM) [26] to *in silico* molecular docking inside *EcFabH* active site. Indeed, comparison of the generated **Cpd23** docking pose with its available binding geometry observed in *EcFabH* crystal structure (PDB entry code: 5BNR; 1.89 Å resolution) revealed a root mean square deviations of 0.622 Å for the top ranked pose with a predicted binding energy value,  $\Delta E_{\text{Cpd23}} = -8.1 \text{ kcal.mol}^{-1}$ . This re-/cross-docking experiment thus confirms the validity and reliability of our computational approach.

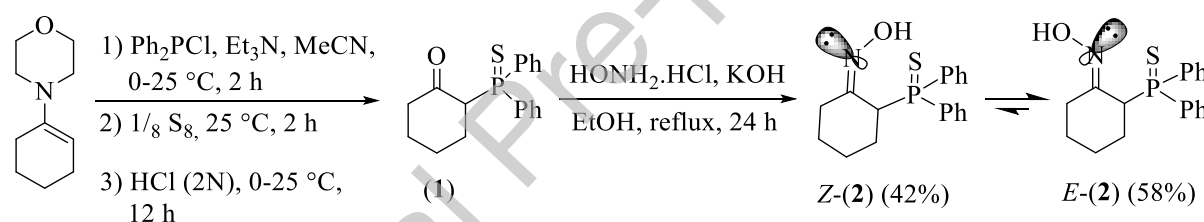


### 3. Results and discussion

#### 3.1. Synthesis of (2-(hydroxyimino)cyclohexyl)diphenylphosphine sulfide (2)

The starting 2-(diphenylphosphorothioyl)cyclohexanone (**1**) was easily prepared from the reaction of a cyclic enamine [1-morpholinocyclohexene] with *P*-chlorodiphenylphosphine in the presence of triethylamine, followed by sulfurization and hydrolytic work-up, according to the reported procedure [27]. Reaction of compound (**1**) with hydroxylamine hydrochloride, performed in refluxing ethanol for 24 h in the presence of an equimolar amount of potassium hydroxide, led to the desired  $\alpha$ -(diphenylphosphorothioyl)cyclohexanone oxime (**2**) in 87% isolated yield (**Scheme 1**).

It is important to mention here that compound (**2**) was obtained as a mixture of *Z* and *E* isomers in 42:58 ratio, as evidenced by its NMR spectral data.



**Scheme 1.** Synthesis of compound (**2**).

#### 3.2. FT-IR, NMR and mass spectrometry studies

The structure of compound (**2**) was confirmed on the basis of its FT-IR,  $^1\text{H}$  NMR,  $^{13}\text{C}$  NMR, and  $^{31}\text{P}$  NMR spectral data. The high-resolution mass spectrum of the studied compound displayed molecular ion peak at appropriate  $m/z$  value.

##### 3.2.1. FT-IR study

Fourier Transform Infrared spectroscopy (FT-IR) is known as a useful quantitative and qualitative analysis tool for both organic and inorganic compounds. Thus, a vibrational study using infrared absorption was performed to gain more insights on the structure, the functional groups and the types of bonding existing in the title compound.

The IR bands of the synthesized compound are assigned by comparison with the modes and frequencies observed in similar derivatives. The experimental FT-IR spectrum of

compound (**2**) (**Fig. S1** in Supplementary Information) revealed the presence of a band at  $3343\text{ cm}^{-1}$  corresponding to the O-H vibrator of the oxime group [28]. We also noticed the presence of absorption bands of medium intensities between  $2991$  and  $2950\text{ cm}^{-1}$  attributed to the stretching vibrations of CH and  $\text{CH}_2$  groups [29]. The absorption band at  $1638\text{ cm}^{-1}$  is assigned to the stretching of the C=N double bond of the oxime group [30]. The bands of medium intensities between  $1374$  and  $1474\text{ cm}^{-1}$  are assigned to the stretching modes of the phenyl C=C double bonds [31]. The absorption at  $698\text{ cm}^{-1}$  is attributed to the stretching of the thiophosphoryl (P=S) group [32]. In the frequency region between  $794$  and  $1174\text{ cm}^{-1}$ , bands of medium intensities are present, which could be assigned to the skeletal C-C vibrations of the cyclohexane ring [33]. The rest of absorptions between  $480$  and  $997\text{ cm}^{-1}$  are attributed to out-of-plane bending modes of C-H bonds [34].

### 3.2.2. NMR study

The  $^{13}\text{C}$ ,  $^{31}\text{P}$ , and  $^1\text{H}$  NMR spectra of the title compound are given in the Supplementary Information. All NMR spectra of compound (**2**) showed a signal doubling indicating that it is obtained as a mixture of *Z* and *E* isomers.

The *Z* and *E* configurations were assigned on the basis of the  $^{13}\text{C}$  chemical shifts of carbons in  $\alpha$  position with respect to the C=N double bond. Indeed, according to some literature data regarding the stereochemistry of oximes [35], the carbon adjacent to the C=N double bond resonates at higher field when it is in the *syn* position relative to the OH group on the nitrogen atom. This was ascribed to a screening effect of the *syn*-OH group. In our case, The CH carbon adjacent to the C=N double bond is characterized by two doublets at  $34.8\text{ ppm}$  and  $42.2\text{ ppm}$ . Each doublet is characteristic of the coupling with phosphorus with a  $^1J_{\text{CP}}$  coupling constant of  $39.2\text{ Hz}$  and  $42.3\text{ Hz}$  respectively. The first doublet, which appears at higher fields, is assigned to the CH carbon when it is *syn* with respect to the OH group (*Z* isomer). However, the second doublet, which appears at lower fields, is assigned to the CH carbon when it is *anti* to the OH group. This assignment corresponds to the *E* isomer. It is important to note here that the  $^{13}\text{C}$  chemical shifts of the  $\text{CH}_2$  carbon, which is in the  $\alpha'$  position with respect to the C=N double bond, follow the same correlations as the CH carbon atom.

The relative proportions of the *Z* and *E* isomers were estimated from the  $^{31}\text{P}\{^1\text{H}\}$  NMR spectrum where a singlet for each isomer is present. The *E* stereoisomer was found to be the predominant form ( $E/Z = 58:42$ ) probably due to the steric hindrance between the phosphorothioyl and hydroxyl groups, which destabilizes the *Z* isomer. The  $^1\text{H}$  NMR

spectrum of the studied compound showed, in particular, a broad singlet at 9.0 ppm, ascribable to the OH group. It also exhibited the presence of the CH and CH<sub>2</sub> groups of the cyclohexane ring between 1.42 and 4.90 ppm, and the aromatic protons in the range of 7.29-8.18 ppm.

### 3.3. Single crystal X-ray diffraction analysis

Single crystals (colorless crystals) of C<sub>18</sub>H<sub>20</sub>NOPS (**2**) were obtained by slow evaporation at room temperature of a methanol/hexane/ethyl acetate solution. Crystal data and experimental parameters used for the intensity data collection for the studied compound, are summarized in **Table 1**. CCDC 1992904 contain the supplementary crystallographic data for this compound and can be obtained free of charge via [www.ccdc.cam.ac.uk/conts/retrieving.html](http://www.ccdc.cam.ac.uk/conts/retrieving.html) (or from the Cambridge Crystallographic Data Centre, 12, Union Road, Cambridge CB2 1EZ, UK; fax: +44-1223-336033; or [deposit@ccdc.cam.ac.uk](mailto:deposit@ccdc.cam.ac.uk)).

**Table 1.** Crystallographic data and structure refinement parameters for compound (**2**).

Empirical formula	C <sub>18</sub> H <sub>20</sub> NOPS
Formula weight [g mol <sup>-1</sup> ]	329.38
Temperature (K)	100(1)
Wavelength	1.54184
Crystal system	Monoclinic
Space group	P21/c
a [Å]	15.66750(10)
b [Å]	9.21860(10)
c [Å]	12.40990(10)
α (°)	90
β (°)	110.9130(10)
γ (°)	90
V (Å <sup>3</sup> )	1674.32(3)
Z	4
ρ <sub>calc</sub> [g cm <sup>-3</sup> ]	1.307
Absorption coefficient μ [mm <sup>-1</sup> ]	1 2.618
F(000)	696.0
Crystal size (mm <sup>3</sup> )	0.247 × 0.14 × 0.055
2 θ range [°]	6.038 to 147.732
h, k, l ranges	9, 28, 11
Reflections collected	30497
Independent reflections [R <sub>int</sub> ]	3382

Completeness to $\theta$	98.7%
Refinement method	Full-matrix least squares on $F^2$
Data/restraints/parameters	3382/0/202
Goodness-of-fit on $F^2$	1.043
Final R indices [ $I > 2\sigma(I)$ ]	$R_1 = 0.0275$ , $wR_2 = 0.0718$
R indices (all data)	$R_1 = 0.0304$ , $wR_2 = 0.0742$
Largest diff. peak/hole [ $e \text{ \AA}^{-3}$ ]	0.36/-0.24

Oxime (**2**) was found to crystallize in the monoclinic system with centrosymmetric  $P2_1/c$  space group (**Table 1**). A perspective view of the asymmetric unit of the structure of (**2**) with 50% probability thermal ellipsoids is depicted in **Fig. 1**. It consists of a diphenylphosphorothioyl moiety linked to a cyclohexanone oxime ring in position 2.

The title compound crystallized as the *E* isomer, although this material gave an *E/Z* ratio of 58:42 in  $CDCl_3$  solution as mentioned by NMR spectroscopy. This could be ascribed to crystal lattice forces overcoming the *E/Z* energy difference which was calculated as  $4.7 \text{ kcal.mol}^{-1}$  in favor of the *E* isomer (see paragraph 3.4).

The molecule exhibits a regular spatial configuration with usual distances and angles (**Table 2** and **Fig. 1**). The dihedral angle between the two phenyl groups on the phosphorus atom is  $105.03^\circ$ , showing a quasi-orthogonal arrangement of the two phenyl rings due to steric reasons. The P-S distance of  $1.9559(4) \text{ \AA}$  is consistent with a P-S double bond.

The cyclohexanone oxime ring is in the characteristic chair conformation and its geometrical parameters are reported in Table 2 indicating that the C-C and C-N distances as well as the C-C-C and C-C-N angles are in accordance with those observed in similar compounds [36-41]. The conformation of the cyclohexanone oxime six-membered ring can be described in terms of Cremer and Pople puckering coordinates [42], *i.e.*, evaluating the parameters  $Q$  (total puckering amplitude),  $q_2$ ,  $q_3$ ,  $\theta$  and  $\varphi$ . Their calculated values for the C1-C2-C3-C4-C5-C6 ring are:  $Q = 0.5974 \text{ \AA}$ ,  $q_2 = 0.0518 \text{ \AA}$ ,  $q_3 = 0.5952 \text{ \AA}$ ,  $\theta = 4.98^\circ$  and  $\varphi = 56.85^\circ$ , indicating that the cyclohexanone oxime ring has been slightly distorted from the standard chair conformation by the oxime group.

**Table 2.** Bond lengths [ $\text{\AA}$ ] and angles [ $^\circ$ ] for compound (2).

Selected bond Lengths							
Atom	Atom	Length[ $\text{\AA}$ ]	Atom	Atom	Length[ $\text{\AA}$ ]		
P1	S1	1.9559(4)	C7	C12	1.3904(19)		
P1	C1	1.8297(12)	C8	C9	1.389(2)		
P1	C7	1.8255(13)	C9	C10	1.384(2)		
P1	C13	1.8137(13)	C10	C11	1.380(2)		
C1	C2	1.5110(16)	C11	C12	1.392(2)		
C1	C6	1.5463(17)	C13	C14	1.3923(18)		
C2	C3	1.5030(17)	C13	C18	1.4003(18)		
C2	N1	1.2782(16)	C14	C15	1.3879(19)		
C3	C4	1.5354(18)	C15	C16	1.386(2)		
C4	C5	1.5293(17)	C16	C17	1.3913(19)		
C5	C6	1.5327(17)	C17	C18	1.391(4)		
C7	C8	1.3913(19)	O1	N1	1.4147(13)		
Selected Angles							
Atom	Atom	Atom	Angle [ $^\circ$ ]	Atom	Atom	Atom	Angle [ $^\circ$ ]
S1	P1	C1	116.32(4)	C8	C7	P1	119.50(10)
S1	P1	C7	111.29(4)	C12	C7	P1	121.19(10)
O1	P1	C13	110.71(12)	C12	C7	C8	119.22(12)
C2	N1	O1	111.42(10)	C9	C8	C7	120.49(13)
C7	P1	C1	101.49(6)	C10	C9	C8	119.92(14)
C7	P1	C13	105.03(6)	C11	C10	C9	120.01(13)
C13	P1	C1	106.66(6)	C10	C11	C12	120.29(14)
C2	C1	P1	118.24(9)	C7	C12	C11	120.06(14)
C2	C1	C6	107.46(10)	C14	C13	P1	118.40(10)
C6	C1	P1	111.26(8)	C14	C13	C18	119.42(12)
C3	C2	C1	113.06(10)	C18	C13	P1	122.05(10)
N1	C2	C1	119.82(11)	C15	C14	C13	120.30(13)
N1	C2	C3	126.46(11)	C16	C15	C14	120.19(13)
C2	C3	C4	107.27(10)	C17	C16	C15	119.91(13)
C5	C4	C3	111.29(10)	C16	C17	C18	120.33(13)

C6	C5	C4	112.09(11)	C17	C18	C13	119.82(13)
C5	C6	C1	110.44(10)				

The crystal Packing of the title compound showed that the molecules are interconnected via O-H...N intermolecular hydrogen bonds to form dimers of C<sub>18</sub>H<sub>20</sub>NOPS units extending parallel to the crystallographic *b*-axis (**Fig. 2**), with H1...N1 distance of 2.865 Å (**Table 3**). The packing is further stabilized by several H...O, H...S, H...N, H...H, H...C, O...N and O...S interactions with the distances between 2.3 and 3.0 Å (**Fig. 3**), and by weak CH... $\pi$  intermolecular interactions: the distances H6...Cg1 and H1...Cg1 (Cg1 is the centroid of the C7-C8-C9-C10-C11-C12 phenyl ring) are 3.358 and 3.785 Å respectively. The distances from hydrogens H3 and H12 to the centroid Cg2 (Cg2 is the centroid of the C13-C14-C15-C16-C17-C18 phenyl ring) are 3.461 and 3.344 Å respectively (**Fig. 4**).

**Table 3.** Hydrogen-bond geometry (Å, °) for compound (2).

<i>D</i> —H... <i>A</i>	<i>D</i> —H	H... <i>A</i>	<i>D</i> ... <i>A</i>	<i>D</i> —H... <i>A</i>
C3—H3B...O1 <sup>(1)</sup>	0.990	2.692	2.277	103.85
C8—H8...S1 <sup>(1)</sup>	0.950	3.347	3.487 (2)	112.80
C14—H14...S1 <sup>(1)</sup>	0.950	3.424	2.951	112.13
C1—H1A...S1 <sup>(2)</sup>	1.000	3.733	2.743	170.36
C4—H4B...N1 <sup>(3)</sup>	0.990	3.667	2.856	139.68
C5—H5A...O1 <sup>(3)</sup>	0.990	3.500	2.785	129.60
C3—H3A...O1 <sup>(3)</sup>	0.990	3.569	2.902	125.52
C4—H4B...O1 <sup>(3)</sup>	0.990	3.400	2.864	114.77
O1—H1...N1 <sup>(4)</sup>	0.831	2.865	2.084	156.48
O1—H1...S1 <sup>(4)</sup>	0.831	3.282	2.861	113.48
O1—H1...O1 <sup>(4)</sup>	0.831	3.258	2.703	125.67
C16—H16...S1 <sup>(5)</sup>	0.950	3.844	2.957	156.03

Symmetry codes: (1) *x*,*y*,*z*; (2) *x*,*-y*+1/2,*z*+1/2; (3) *-x*+1,*y*+1/2,*-z*+1/2+1; (4) *-x*+1,*-y*+1,*-z*+1; (5) *x*,*-y*+1/2,*z*+1/2.

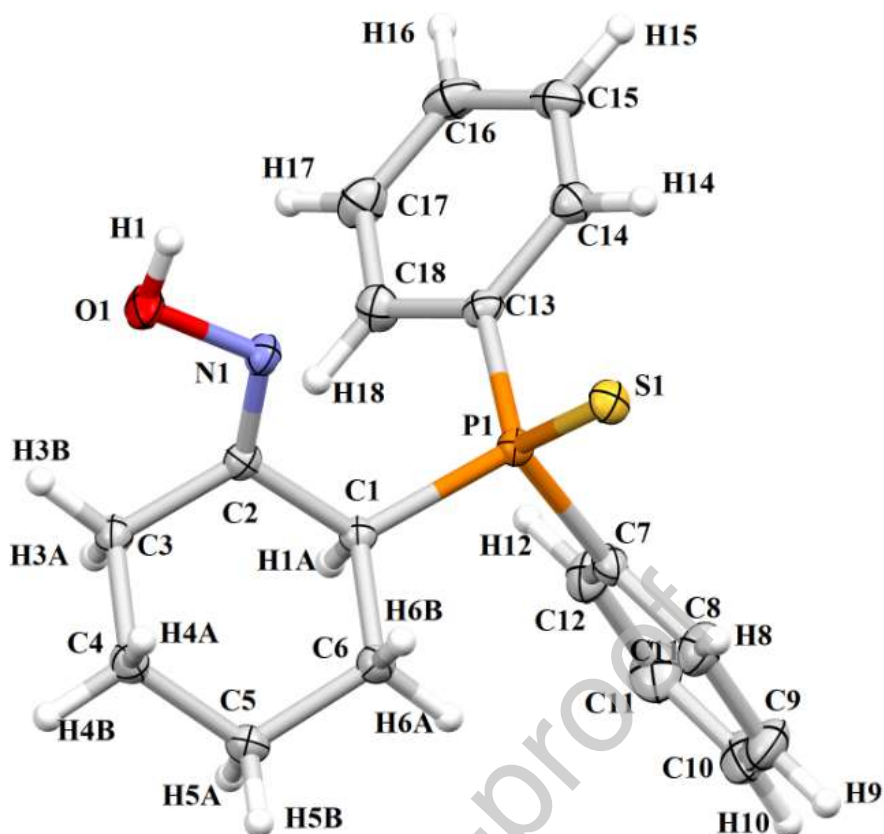


**Figure 1.** X-ray molecular structure of compound (2) with the atom numbering scheme. Displacement ellipsoids are drawn at the 50% probability level.

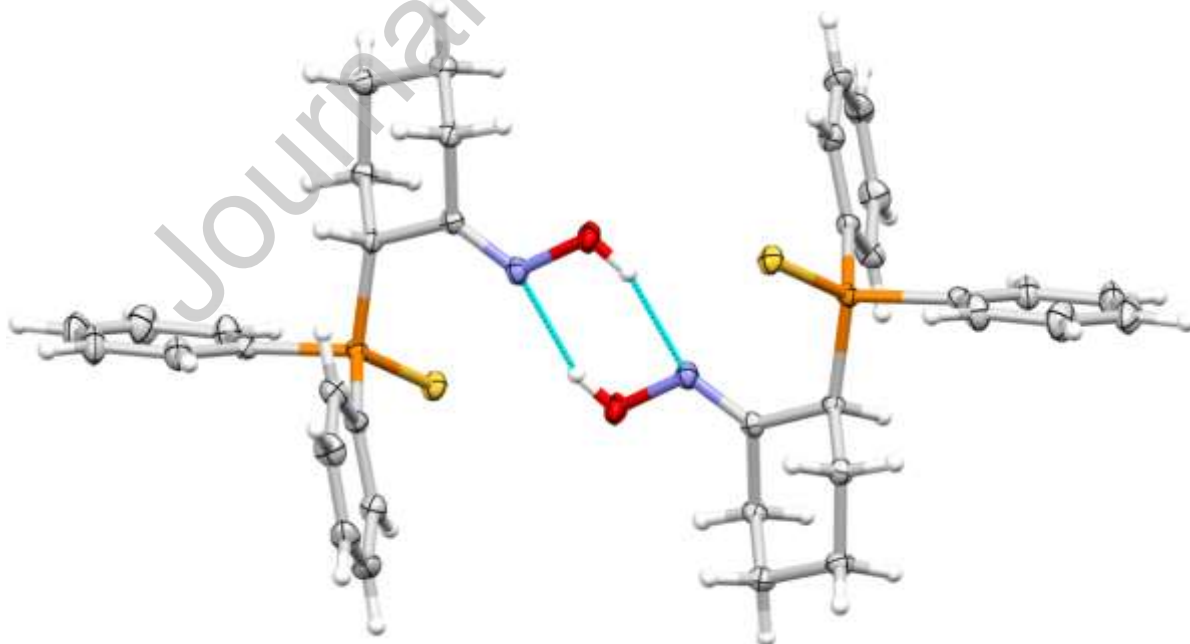


**Figure 2.** The hydrogen-bonded dimer structure of (2) in an *E* configuration, formed *via* intermolecular O-H...N.

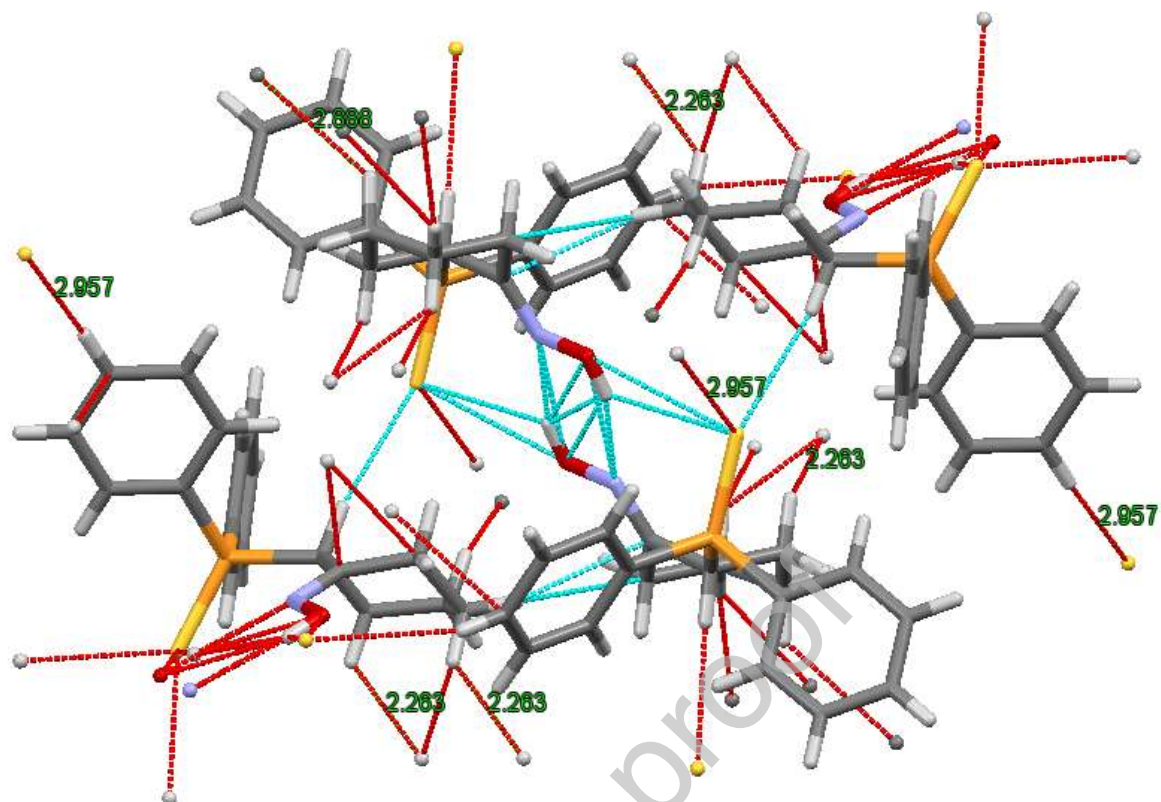


**Figure 3.** A projection along the a-axis showing various short interactions in the crystal packing of (2).

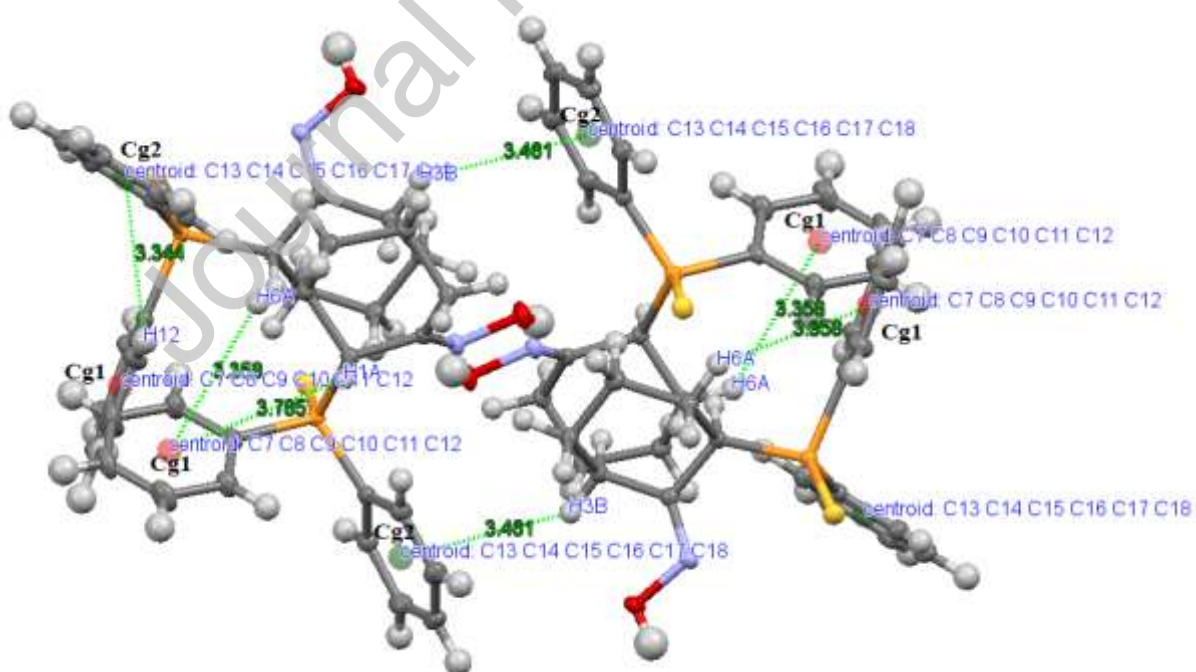


**Figure 4.** Illustration of C-H... $\pi$  intermolecular interactions in  $C_{18}H_{20}NOPS$  crystal.



### 3.4. DFT calculations

In order to get more insights into the *Z/E* isomerism of oxime (**2**) and to obtain additional validations for experimental results, density functional theory (DFT) calculations were performed. The geometries of the *Z* and *E* isomers of compound (**2**) were optimized at the B3LYP/6-311++G(d,p) level of theory both in the gas phase and in a simulated CHCl<sub>3</sub> solvent field (**Fig. S2** in Supplementary Information). The respective relative energies are given in **Table 4**. Our calculations predict the *E* isomer to be preferred by 4.5 kcal.mol<sup>-1</sup> in the gas phase. In a simulated chloroform environment, it remains the most stable isomer by 4.7 kcal.mol<sup>-1</sup>, in agreement with the *E/Z* ratio of 58:42 determined by NMR spectroscopy in CDCl<sub>3</sub> solution. Such a predominance of the *E* isomer could be ascribed to the steric hindrance between the phosphorothioyl and hydroxyl groups, which may destabilize the *Z* isomer.

DFT calculations also play an important role in predicting the biological activity of compounds and drugs [43]. It is indeed well established that a molecule with a smaller LUMO-HOMO energy gap is considered as more chemically reactive and therefore more energetically favorable to extract electrons from a high-lying HOMO or to add electrons to a low-lying LUMO, which leads to a better interaction with the target enzyme and consequently to a higher biological activity [43].

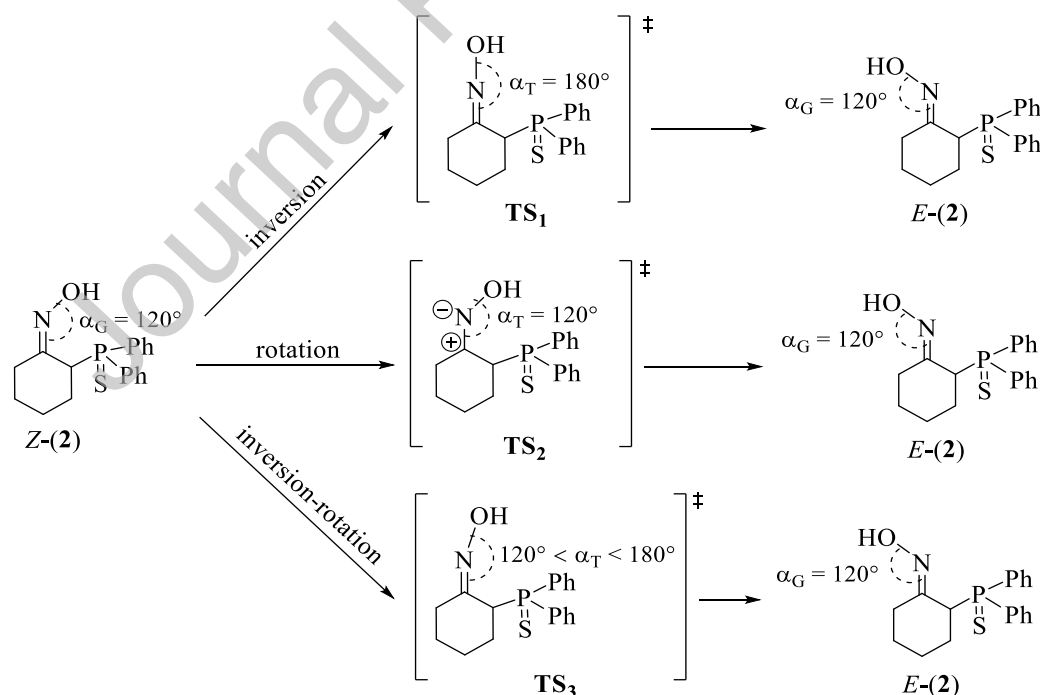
We have recently reported that compound (**2**), as a mixture of *Z* and *E* isomers, exhibited very promising antibacterial activity against both Gram-positive and Gram-negative bacteria [12]. Here, we attempted to compare the antibacterial activities of both *Z* and *E* isomers of (**2**) in correlation with their LUMO-HOMO energy gap. It should be mentioned that, despite our efforts, we were unable to separate and isolate these two isomers, and therefore a direct determination of their respective antibacterial activities, based on *in vitro* tests, was not possible.

The results of DFT calculations, both in the gas phase and in a simulated chloroform environment (**Table 4** and **Fig. S3** in Supplementary Information), revealed that the *Z*-(**2**) isomer has the smaller LUMO-HOMO energy gap, indicating a predicted better antibacterial activity than *E*-(**2**) isomer. Such results could explain the general tendency observed in our previous study on similar compounds [12], showing that oximes more rich in *Z* isomer exhibited a better antibacterial activity.

**Table 4.** Relative energies and frontier molecular orbitals (HOMO and LUMO) energies for the *Z* and *E* isomers of compound (**2**) both in the gas phase and in a simulated CHCl<sub>3</sub> solution.

Isomers	Relative energies (kcal.mol <sup>-1</sup> )	E <sub>HOMO</sub> (eV)	E <sub>LUMO</sub> (eV)	ΔE <sub>LUMO-HOMO</sub> (eV)
<i>E</i> -( <b>2</b> ) (gas)	0	-5.8732	-1.2564	4.6168
<i>Z</i> -( <b>2</b> ) (gas)	4.5	-5.8536	-1.2531	4.6005
<i>E</i> -( <b>2</b> ) (CHCl <sub>3</sub> )	0	-6.2220	-1.3486	4.8734
<i>Z</i> -( <b>2</b> ) (CHCl <sub>3</sub> )	4.7	-6.1948	-1.3454	4.8494

We then turned our attention to investigate, through DFT-transition state calculations, the mechanism of *Z/E* isomerization in oxime (**2**). A literature survey showed that the mechanisms for this kind of isomerization vary depending on the nature of substituents on the C=N double bond [44]. Based on these literature data, we have proposed three possible mechanisms for the *Z/E* isomerization of oxime (**2**), which involve either the nitrogen inversion, or the rotation around the C<sup>+</sup>-N single bond, or a mixed inversion-rotation mechanism (**Scheme 2**).

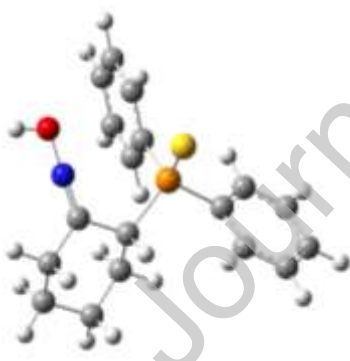
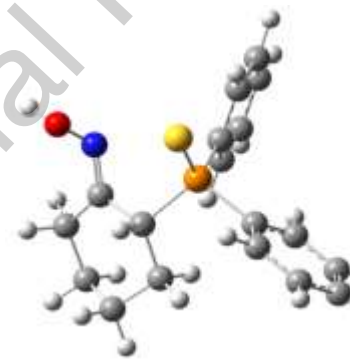
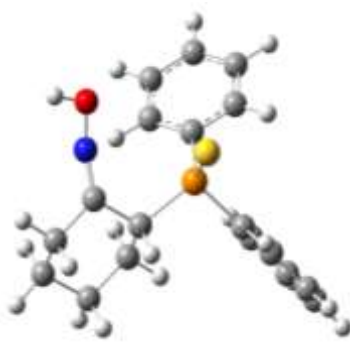


**Scheme 2.** Possible mechanisms, inversion, rotation, or mixed inversion-rotation, for the *Z/E* isomerization of oxime (**2**);  $\alpha_G$  and  $\alpha_T$  are the CNO bond angles in the ground and transition states (TS), respectively.

Fully optimized structures of the ground states [*Z*-(**2**) and *E*-(**2**)] and transition states [**TS**<sub>1</sub>, **TS**<sub>2</sub> and **TS**<sub>3</sub>] and the corresponding activation energies, were determined at the B3LYP/6-311++G(d,p) level of theory in the gas phase (**Table 5**). Vibrational analyses confirmed that *Z*-(**2**) and *E*-(**2**) isomers have zero imaginary frequencies, and that transition states are true first-order saddle points on the potential energy surface. Intrinsic reaction coordinate (IRC) calculations [45] were followed to check the energy profiles connecting each transition state, through a vibration analysis, to the expected *Z* and *E* forms (**Fig.5**).

The **TS**<sub>1</sub> was found to be more stable than **TS**<sub>2</sub> and **TS**<sub>3</sub> with an activation energy of 41.8 kcal.mol<sup>-1</sup> (**Table 5** and **Fig.5**). Such a predominance of **TS**<sub>1</sub> over the others introduces a clear-cut evidence that the most probable mechanism by which occur the *Z/E* isomerization in compound (**2**) is the nitrogen inversion pathway.

**Table 5.** DFT calculation results for the transition states **TS**<sub>1</sub>, **TS**<sub>2</sub> and **TS**<sub>3</sub> obtained during the *Z/E* isomerization of oxime (**2**) through either inversion, or rotation, or a mixed inversion-rotation mechanism.

Inversion	Rotation	Inversion-rotation
		
<b>TS</b> <sub>1</sub> structure	<b>TS</b> <sub>2</sub> structure	<b>TS</b> <sub>3</sub> structure
$Ea_1 = 41.8 \text{ kcal.mol}^{-1}$	$Ea_2 = 55.0 \text{ kcal.mol}^{-1}$	$Ea_3 = 46.4 \text{ kcal.mol}^{-1}$
$\alpha_T^1 = 177.4^\circ$	$\alpha_T^2 = 120.0^\circ$	$\alpha_T^3 = 150.0^\circ$
$\alpha_G^1 = 123.3^\circ$	$\alpha_G^2 = 119.4^\circ$	$\alpha_G^3 = 123.1^\circ$
$d_{C=N} = 1.246 \text{ \AA}$	$d_{C=N} = 1.299 \text{ \AA}$	$d_{C=N} = 1.264 \text{ \AA}$

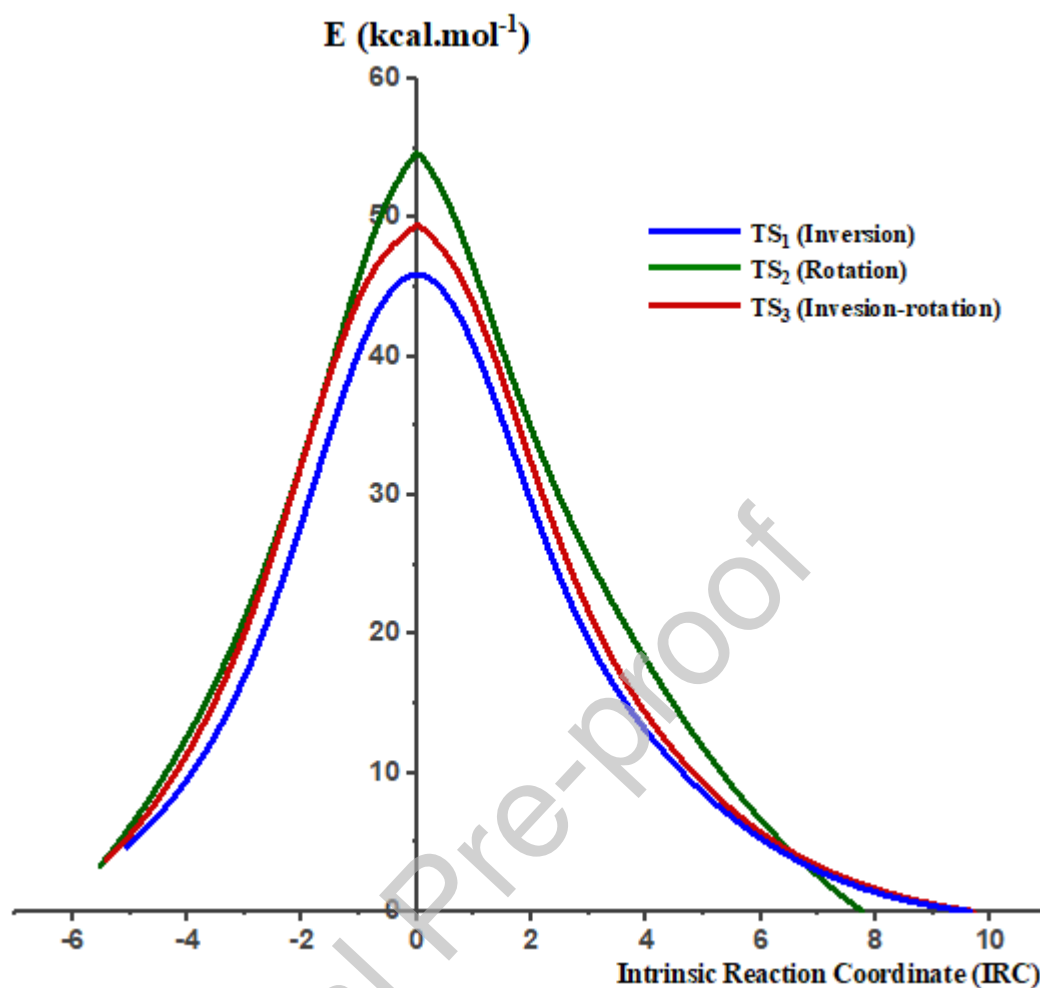


**Figure 5.** IRC plots for the transition states  $TS_1$ ,  $TS_2$  and  $TS_3$  obtained during the  $Z/E$  isomerization of oxime (**2**) through either inversion, or rotation, or a mixed inversion-rotation mechanism.

### 3.5. *In silico* molecular docking study

With the aim to corroborate the predicted biological activity derived from DFT calculations, *in silico* molecular docking studies in *E. coli*  $\beta$ -ketoacyl-acyl carrier protein synthase III (*EcFabH*) enzyme active site were performed. *FabH* catalyzes the first condensation step between acetyl-CoA and malonyl-ACP thus initiating the fatty acid elongation cycles [46], and has been validated as an attractive drug target [47]. Moreover, *FabH* inhibitors are distinguished because their target is different from that of common antibacterial drugs. Therefore, discovery of novel *FabH* inhibitors might be a potential orientation to overcome bacterial resistance. Given the fact that oxime derivatives have been shown to inhibit *EcFabH* [23, 47], *in silico* molecular docking experiments were conducted

as described previously with cycloalkanone oxime analogues of compound (**2**) [12], on both *Z*-(**2**) and *E*-(**2**) isomers to predict and compare their possible interaction modes and binding energies, using the reported crystal structure of *E. coli* FabH (*EcFabH*) (PDB entry code: 1HNJ) [25].

Consistent with our previous docking results obtained with cyclopentanone oxime compounds [12], the best scoring position obtained (*i.e.*, lowest energy complex) showed that *Z*-(**2**) and *E*-(**2**) isomers would be located at the right entrance of the catalytic cleft of the *EcFabH* active site. Moreover, in both cases, the docked isomers would also be positioned at a distance  $>9$  Å from the catalytic Cys<sup>112</sup>, thus excluding any covalent interaction (**Figs. 6A** and **7A**). Remarkably, these two isomers displayed different and clearly distinct predicted binding energy values. With a  $\Delta E_{Z-(2)} = -6.8$  kcal.mol<sup>-1</sup>, the *Z* isomer would therefore exhibit a better affinity for the *EcFabH* active site than the *E* isomer ( $\Delta E_{E-(2)} = -6.1$  kcal.mol<sup>-1</sup>).

In order to schematically depict the hydrogen bonds and hydrophobic interactions between the ligand (*i.e.*, *Z*-(**2**) or *E*-(**2**) isomer), and the active site residues of *EcFabH* during the binding process, each of the docked *Z*-(**2**)-*EcFabH* and *E*-(**2**)-*EcFabH* complexes was further subjected to interactions analysis using Ligplot+ v.1.4 [48]. In the obtained binding model (**Fig. 6B**), the two bulky phenyl groups of *Z*-(**2**) may be involved in  $\pi$ -stacking interactions with Trp<sup>32</sup>, GLy<sup>152</sup>, Ile<sup>156</sup>, Met<sup>207</sup>, Gly<sup>209</sup> and Asn210, while the cyclohexanone oxime moiety would be stabilized by 2 H-bonding with Arg<sup>36</sup> and Asn<sup>247</sup> residues and interact with Thr<sup>37</sup>, Phe<sup>213</sup> and Arg<sup>249</sup> residues (**Fig. 6B**).

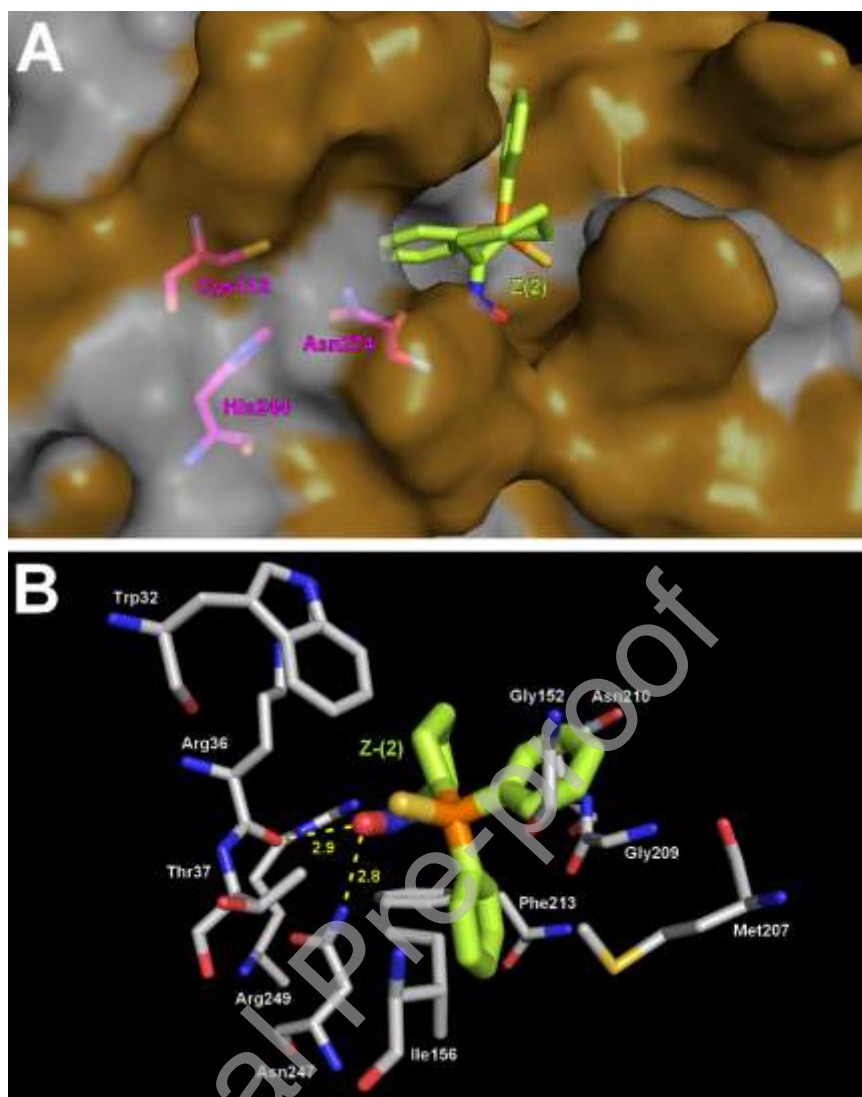


**Figure 6.** (A) *In silico* molecular docking of the Z-(2) isomer (yellow color) into the crystallographic structure of *E. coli* FabH in a van der Waals surface representation. The Cys<sup>112</sup>-His<sup>244</sup>-Asn<sup>274</sup> catalytic residues of *EcFabH* active site are in magenta stick representation. Hydrophobic residues (alanine, leucine, isoleucine, valine, tryptophan, tyrosine, phenylalanine, proline, and methionine) are highlighted in white. (B) Ligplot+ analyses results: 3D representation of the schematic binding mode of Z-(2) (yellow color) in complex with *EcFabH* showing both hydrogen bonds (yellow dashed lines) and hydrophobic interactions. Selected residues of the *EcFabH* binding pocket are shown as gray sticks. The stick representation uses the following atom color-code: nitrogen, blue; oxygen, red; sulfur, yellow; and phosphorus, orange. Structures were drawn with PyMOL Molecular Graphics System (version 1.4, Schrödinger, LLC) using the PDB file 1HNJ [25].

As depicted in **Fig. 7A,B**, the highest-scoring productive docking positions of *E*-(**2**) led to two concurrent and opposite binding modes resulting from a rotation around the Ph-P=S axis, *i.e.*, *E*-(**2**)<sub>1</sub> and *E*-(**2**)<sub>2</sub> (**Fig. 7B**) with the same predicted binding energy value. Interestingly, despite an opposite orientation of the N-OH due to the *Z/E* isomerization, the binding mode of *E*-(**2**)<sub>1</sub> is closely superimposable with that of the *Z*-(**2**) isomer, and also subjected to similar hydrophobic interactions with two H-bonding involving Arg<sup>36</sup> and Arg<sup>249</sup> residues (**Fig. 7C**). In contrast, no Hydrogen bond was detected in *E*-(**2**)<sub>2</sub> productive orientation, where only hydrophobic interactions were observed (**Fig. 7D**). Such discrepancy between the two binding modes of the *E* isomer might be a possible explanation for the less good predicted binding energy obtained.

In a way to correlate these docking results with the potential respective inhibitory activity of *Z*-(**2**) and *E*-(**2**) isomers towards *EcFabH*, the (*E*)-*N*-((3,4-dihydro-2*H*-benzo[*b*][1,4]dioxepin-7-yl)methylene)-hexadecan-1-amine (*i.e.*, **Cpd10**), which is a potent inhibitor of *EcFabH* (IC<sub>50</sub> = 1.6 μM) [23c], was also docked in the enzyme active site (**Fig. S4** in Supplementary Information). In this case, the highest-scoring productive docking positions led to two reverse binding modes, mainly stabilized by hydrophobic interactions (**Fig. S4** in Supplementary Information), and exhibiting the same predicted binding energy  $\Delta E_{\text{Cpd10}} = -6.0 \text{ kcal.mol}^{-1}$ . Noteworthy, a pretty good level of concordance between these two favorable docked conformations of **Cpd10** and the crystal structure of the **Cpd23**-*EcFabH* (PDB entry code: 5BNR) [26] was also observed (**Fig. S4B** in Supplementary Information).

Overall, this docking study with both *Z*-(**2**) and *E*-(**2**) isomers strongly suggest that the *Z* isomer would be able to block the access of the substrate into the *EcFabH* protein's active site, therefore resulting in a more efficient predicted inhibitory activity than the *E* isomer, and even maybe better than **Cpd10**, used here as reference inhibitor.

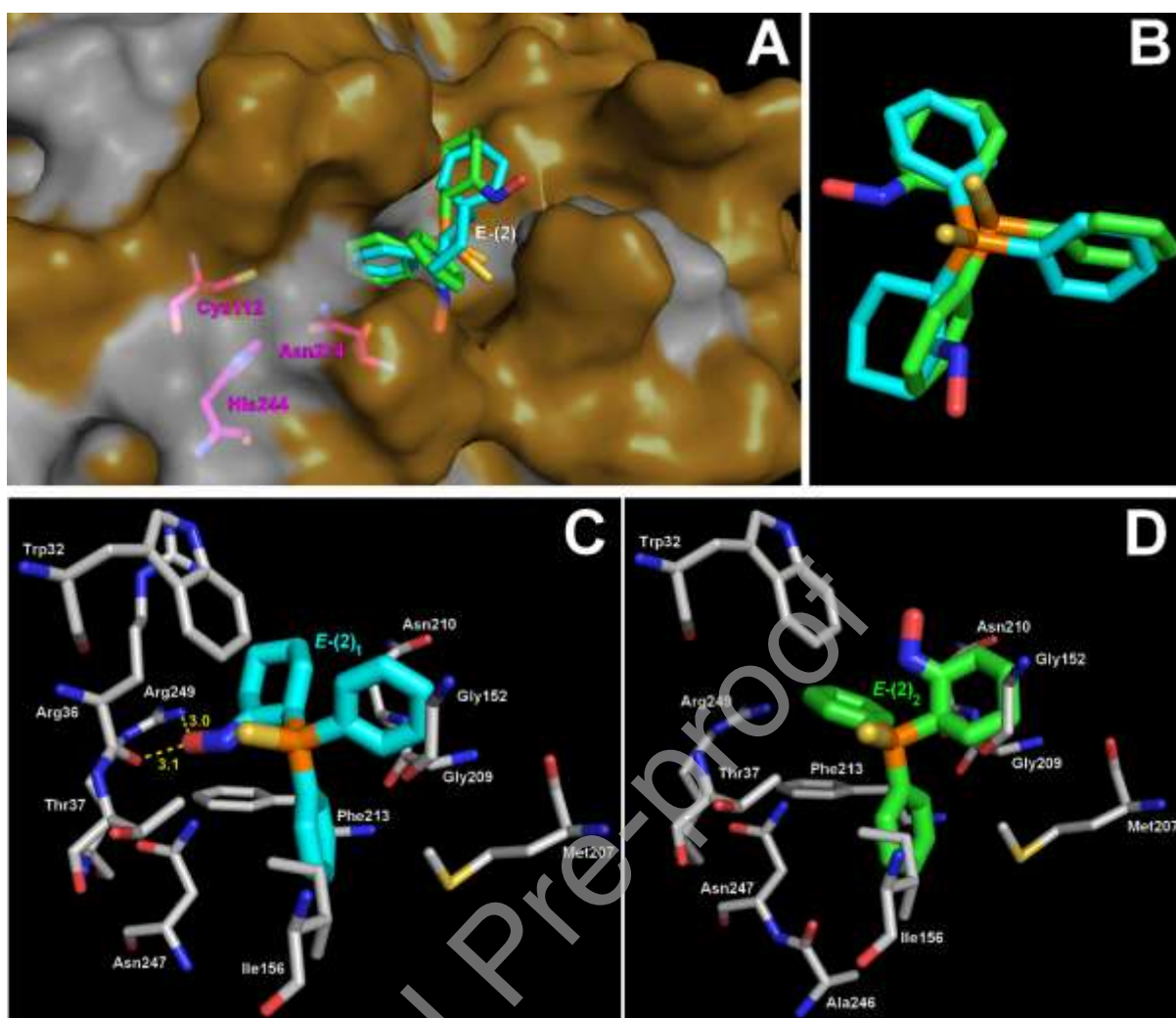


**Figure 7.** (A) *In silico* molecular docking of the *E*-(2) isomer into the crystallographic structure of *E. coli* FabH in a van der Waals surface representation. The Cys<sup>112</sup>-His<sup>244</sup>-Asn<sup>274</sup> catalytic residues of *Ec*FabH active site are in *magenta stick* representation. Hydrophobic residues (alanine, leucine, isoleucine, valine, tryptophan, tyrosine, phenylalanine, proline, and methionine) are highlighted in *white*. (B) Superimposition of the two equally scoring binding modes obtained, *i.e.*, *E*-(2)<sub>1</sub> (*cyan color*) and *E*-(2)<sub>2</sub> (*green color*). (C-D) Ligplot+ analyses results: 3D representation of the schematic binding mode of *E*-(2)<sub>1</sub> (C; *cyan color*) and *E*-(2)<sub>2</sub> (D; *green color*) in complex with *Ec*FabH showing both hydrogen bonds (*yellow dashed lines*) and hydrophobic interactions. Selected residues of the *Ec*FabH binding pocket are shown as *gray sticks*. The stick representation uses the following atom color-code: nitrogen, blue; oxygen, red; sulfur, yellow; and phosphorus, orange. Structures were drawn with PyMOL Molecular Graphics System (version 1.4, Schrödinger, LLC) using the PDB file 1HNJ [25].



## 4. Conclusion

The molecular structure of a novel phosphorus-containing oxime [(2-(hydroxyimino)cyclohexyl)diphenylphosphine sulfide, C<sub>18</sub>H<sub>20</sub>NOPS (**2**)] was studied by using various spectroscopic tools including FT-IR, NMR (<sup>1</sup>H, <sup>31</sup>P, <sup>13</sup>C), mass spectrometry and single crystal X-ray diffraction. The title compound was found to crystallize as the *E* isomer, but this material equilibrates in CDCl<sub>3</sub> solution to give an *E/Z* ratio of 58:42, corresponding to an energy difference of 4.7 kcal.mol<sup>-1</sup> in favor of the *E* isomer. The different mechanisms, inversion, rotation, or mixed inversion-rotation, by which could occur the *Z/E* isomerization, have been investigated computationally through DFT-transition state calculations, showing that the most probable mechanism for this isomerization is the nitrogen inversion pathway. The antibacterial activities of the *Z* and *E* isomers were compared, theoretically, in correlation with their LUMO-HOMO energy gap. The results of DFT calculations, both in the gas phase and in a simulated chloroform environment, showed that the *Z* isomer has the smaller LUMO-HOMO energy gap, indicating a better antibacterial activity than *E* isomer. This was corroborated by *in silico* molecular docking studies in *EcFabH* enzyme active site which also showed that the *Z* isomer exhibited a better predicted inhibitory activity than the *E* isomer, and even maybe better than **Cpd10**, used here as reference inhibitor. Encouraged by these results, other studies on the structural modification of such phosphorus-containing oximes, in order to obtain additional analogues enriched in *Z* isomer, are ongoing in our laboratory and will be reported in due course. This might further enhance the antibacterial activity of these pharmacophores.

## Acknowledgement

The authors are grateful to the Tunisian Ministry of Higher Education and Scientific Research for financial support.

## Supplementary material

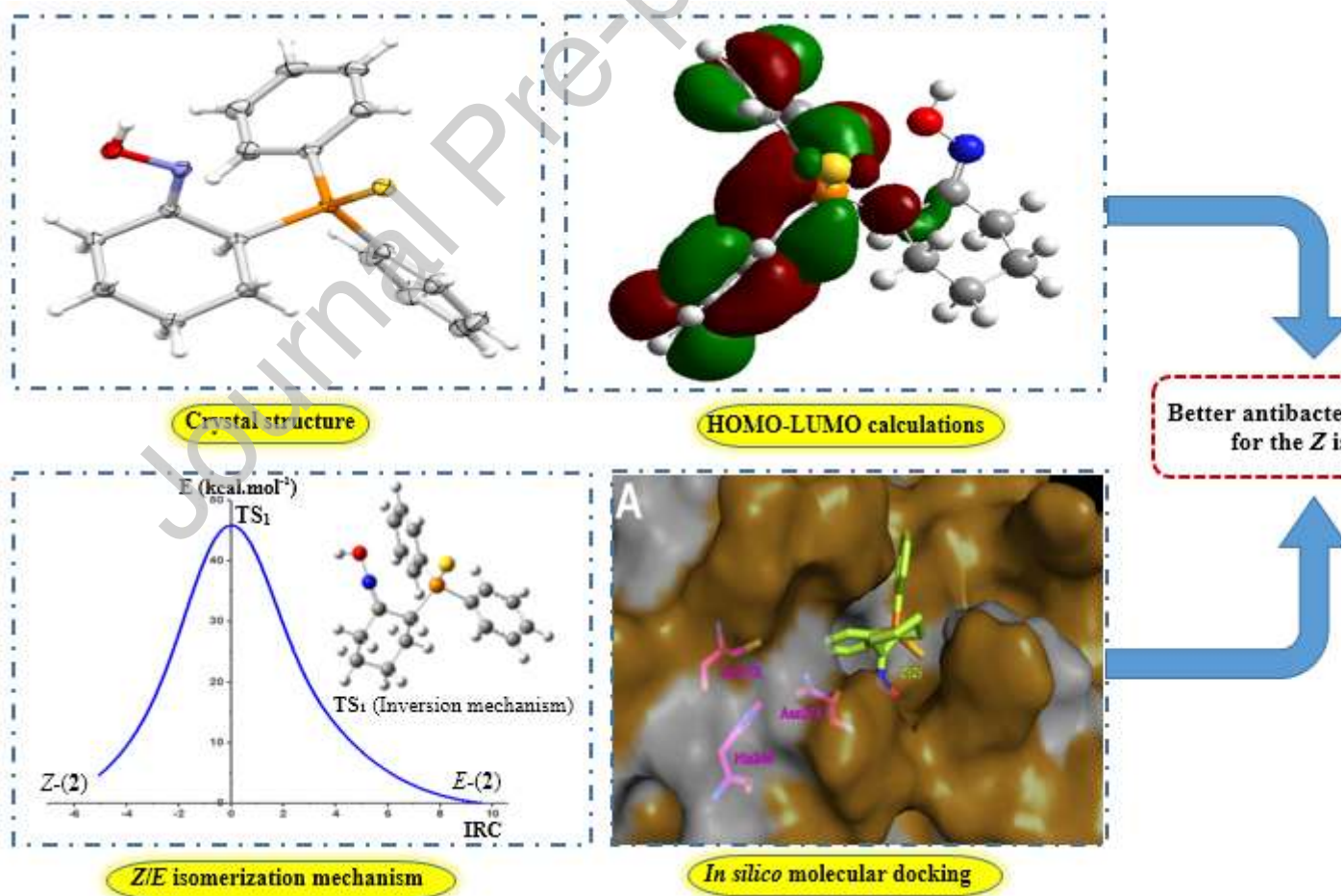
Supplementary data related to this article can be found at <http://dx.doi.org/10.1016/j.molstruc>.

**Credit Author Statement**

N. Jebli synthesized the compounds and analyzed the data. Y. Arfaoui conducted the theoretical calculations. K.V. Hecke performed the X-ray diffraction analysis. J-F. Cavalier carried out the *in silico* molecular docking studies. S. Touil designed and supervised the work and analyzed the data.

**Declaration of interests:**

The authors declare that there are no conflicts of interests.

**Graphical Abstract:**

## References

- [1] (a) E. Abele, R. Abele, E. Lukevics, Pyridine Oximes: Synthesis, Reactions, and Biological Activity, *Chem. Heterocycl. Compd.* **39** (2003) 825-865. (b) B. Clement, Reduction of N-hydroxylated compounds: amidoximes (N-hydroxyamidines) as prodrugs of amidines, *Drug Metab. Rev.* **34** (2002) 565-579. (c) P. Parthiban, S. Kabilan, V. Ramkumar, Y.T. Jeong, Stereocontrolled facile synthesis and antimicrobial activity of oximes and oxime ethers of diversely substituted bispidines, *Bioorg. Med. Chem. Lett.* **20** (2010) 6452-6458. (d) S. Emami, M. Falahati, A. Banifatemi, A. Shafiee, Stereoselective synthesis and antifungal activity of (Z)-trans-3-azolyl-2-methylchromanone oxime ethers, *Bioorg. Med. Chem.* **12** (2004) 5881-5889.
- [2] (a) L. Letendre, J. Harriman, M. Drag, A. Mullins, T. Malinski, S. Rehbein, The intravenous and oral pharmacokinetics of afoxolaner and milbemyacin oxime when used as a combination chewable parasiticide for dogs, *J. Vet. Pharmacol. Ther.* **40** (2017) 35-43. (b) T.J. Nolan, J.B. Lok, Macrocyclic lactones in the treatment and control of parasitism in small companion animals, *Curr. Pharm. Biotechnol.* **13** (2012) 1078-1094.
- [3] B. Bednarczyk-Cwynar, L. Zaprutko, Recent advances in synthesis and biological activity of triterpenic acylated oximes, *Phytochem. Rev.* **14** (2015) 203-231.
- [4] F.R. Benn, P.T. Charlton, G.L.M. Harmer, *British Patent* 895495, *Chem. Abstr.* **57** (1962) 13673b.
- [5] A.H. Banday, S.M. Akram, S.A. Shameem, Benzylidene pregnenolones and their oximes as potential anticancer agents: Synthesis and biological evaluation, *Steroids*, **84** (2014) 64-69.
- [6] A. Nikitjuka, A. Jirgensons, Synthesis, Chemical and Biological Properties of Aziridine-1-carbaldehyde Oximes, *Chem. Heterocycl. Compd.* **49** (2014) 1544-1559.
- [7] (a) R. Odzak, C. Maja, H. Tomica, P. Ines, K. Zrinka, Evaluation of monoquaternary pyridinium oximes potency to reactivate tabun-inhibited human acetylcholinesterase, *toxicology.* **233** (2007) 85-96. (b) M. Jokanović, M. Maksimović, V. Kilibarda, D. Jovanović, D. Savić, Oxime-induced reactivation of acetylcholinesterase inhibited by phosphoramidates, *Toxicol. Lett.* **85** (1996) 35-39. (c) J. Stenzel, F. Worek, P. Eyer, Preparation and characterization of dialkylphosphoryl-obidoxime conjugates, potent anticholinesterase derivatives that are quickly hydrolyzed by human paraoxonase (PON<sub>1</sub><sub>192Q</sub>), *Biochem. Pharmacol.* **74** (2007) 1390-1400.

- [8] (a) K. Witold,; R. Janusz, D. Mateusz, D. Sebastian, Selected Methods for the Chemical Phosphorylation and Thiophosphorylation of Phenols, *Asian J. Org. Chem.* 7 (2018) 314-323. (b) C.M. Sevrain, M. Berchel, H. Couthon, P.A. Jaffrès, Phosphonic acid: preparation and applications, *Beilstein J. Org. Chem.* 13 (2017) 2186-2213. (c) Y. Xiaomin, R.D. James, C.J. Sarath, K.Z. Jun, C. Benjamin, M.G. Benjamin, P.L. David, W.M. William, Diversity and abundance of phosphonate biosynthetic genes in nature, *PNAS*, 110 (2013) 20759-20764.
- [9] (a) A.L. Parkes, I.A. Yule, Hybrid antibiotics - clinical progress and novel designs, *Expert Opin. Drug Discov.* 11 (2016) 665-680. (b) P. Klahn, M. Brönstrup, Bifunctional antimicrobial conjugates and hybrid antimicrobials, *Nat. Prod. Rep.* 34 (2017) 832-885.
- [10] (a) A. Bykowska, R. Starosta, U. K. Komarnicka, Z. Ciunik, A. Kyzioł, K. Guz-Regner, G. Bugla-Płoskon'skac, M. Jez'owska-Bojczuk, Phosphine derivatives of ciprofloxacin and norfloxacin, a new class of potential therapeutic agents, *New J. Chem.* 38 (2014) 1062-1071. (b) R. Starosta, M. Florek, J. Kro'ł, M. Puchalska, A. Kochel, Copper(i) iodide complexes containing new aliphatic aminophosphine ligands and diimines-luminescent properties and antibacterial activity, *New J. Chem.* 34 (2010) 1441-1449. (c) C. Marzano, M. Pellei, F. Tisato and C. Santini, Copper complexes as anticancer agents, *Anti-Cancer Agents, Med. Chem.* 9 (2009) 185-211. (d) K. Nepelchova, J. Kasparova, O. Vrana, O. Novakova, A. Habtemarian, B. Watchman, P.J. Sadler, V. Brabec, DNA Interactions of New Antitumor Aminophosphine Platinum(II) Complexes, *Mol. Pharmacol.* 56 (1999) 20-30. (e) C.F. Shaw, Gold-Based Therapeutic Agents, *Chem. Rev.* 99 (1999) 2589-2600.
- [11] (a) E. Chebil, M. Chamakhi, S. Touil, Novel aminophosphonothiophene derivatives from  $\beta$ -keto- $\delta$ -carbethoxyphosphonates and phosphineoxides, *J. Sulfur Chem.* 32 (2011) 249-256. (b) N. Said, S. Touil, A. Ben Akacha, M.L. Efrit, Reactivite Des  $\alpha$ -Phosphonylketones Dans la Reaction de Gewald: Synthese de Nouveaux Derives de L'aminophosphonothiophene, *Phosphorus Sulfur Silicon Relat. Elem.* 183 (2008) 2726-2733. (c) S. Touil, H. Zantour, Synthesis of New Aminophosphonothiophene Derivatives, *Phosphorus Sulfur Silicon Relat. Elem.* 178 (2003) 353-360. (d) S. Touil, H. Zantour, First Synthesis of  $\gamma,\gamma'$ -Diphosphonylketones and Their Reactivity in the Fischer Reaction, *Phosphorus Sulfur Silicon Relat. Elem.* 177 (2002) 1245-1254.
- [12] N. Jebli, S. Hamimed, K. Van Hecke, J.-F. Cavalier, S. Touil, Synthesis, antimicrobial activity and molecular docking study of novel  $\alpha$ -(diphenylphosphoryl)- and  $\alpha$ -

- (diphenylphosphorothioyl)cycloalkanone oximes, *Chem. Biodivers.* *17* (2020) e2000217.
- [13] G. Stork, A. Brizzolara, H. Landesman, J. Szmuszkowicz, R. Terrell, The Enamine Alkylation and Acylation of Carbonyl Compounds, *J. Am. Chem. Soc.* *85* (1963) 207-222.
- [14] Rigaku Oxford Diffraction (2015). CrysAlis Pro; Rigaku Oxford Diffraction, Yarnton, England.
- [15] O.V. Dolomanov, L.J. Bourhis, R.J. Gildea, J.A.K. Howard, H. Puschmann, A rapid method for quantifying heavy atom derivatives for multiple isomorphous replacement in protein crystallography, *J. Appl. Crystallogr.* *42* (2009) 339-341.
- [16] G.M. Sheldrick, A short history of SHELX, *Acta Crystallogr. Sect. A* *64* (2008) 112-122.
- [17] G.M. Sheldrick, Crystal structure refinement with SHELXL, *Acta Crystallogr. Sect. C* *71* (2015) 3-8.
- [18] K. Brandenburg, Diamond Version 2.0 Impact GbR, Bonn., Germany, 1998.
- [19] C.F. Macrae, P.R. Edgington, P. McCabe, E. Pidcock, G.P. Shields, R. Taylor, M. Towler, J. Vandestreek, Mercury: visualization and analysis of crystal structures, *J. Appl. Crystallogr.* *39* (2006) 453-457.
- [20] M.J. Frisch, G.W. Trucks, H.B. Schlegel, G.E. Scuseria, M.A. Robb, J.R. Cheeseman, G. Scalmani, V. Barone, B. Mennucci, G.A. Petersson, H. Nakatsuji, M. Caricato, X. Li, H.P. Hratchian, A.F. Izmaylov, J. Bloino, G. Zheng, J.L. Sonnenberg, M. Hada, M. Ehara, K. Toyota, R. Fukuda, J. Hasegawa, M. Ishida, T. Nakajima, Y. Honda, O. Kitao, H. Nakai, T. Vreven, J.A. Montgomery, Jr., J.E. Peralta, F. Ogliaro, M. Bearpark, J.J. Heyd, E. Brothers, K.N. Kudin, V.N. Staroverov, T. Keith, R. Kobayashi, J. Normand, K. Raghavachari, A. Rendell, J.C. Burant, S. S. Iyengar, J. Tomasi, M. Cossi, N. Rega, J.M. Millam, M. Klene, J.E. Knox, J.B. Cross, V. Bakken, C. Adamo, J. Jaramillo, R. Gomperts, R.E. Stratmann, O. Yazyev, A.J. Austin, R. Cammi, C. Pomelli, J.W. Ochterski, R.L. Martin, K. Morokuma, V.G. Zakrzewski, G.A. Voth, P. Salvador, J.J. Dannenberg, S. Dapprich, A.D. Daniels, O. Farkas, J.B. Foresman, J.V. Ortiz, J. Cioslowski, and D.J. Fox, Gaussian 09, Revision B.01 Gaussian, Inc., Wallingford CT, (2010).
- [21] R.D. Dennington, T.A. Keith, J.M. Millam, GaussView 5.0.8, *Gaussian Inc.* 2008.

- [22] O. Trott, A.J. Olson, AutoDock Vina: Improving the speed and accuracy of docking with a new scoring function, efficient optimization, and multithreading', *J. Comput. Chem.* 31 (2010) 455-461.
- [23] (a) Y. Zhou, Y. Luo, Y.S. Yang, L. Lu, H.L. Zhu, Study of acylhydrazone derivatives with deoxygenated seven-membered rings as potential  $\beta$ -ketoacyl-acyl carrier protein synthase III (FabH) inhibitors, *Med. Chem. Comm.* 7 (2016) 1980-1987. (b) X.-L. Wang, Y.-B. Zhang, J.-F. Tang, Y.-S. Yang, R.-Q. Chen, F. Zhang, H.-L. Zhu, Design, synthesis and antibacterial activities of vanillic acylhydrazone derivatives as potential  $\beta$ -ketoacyl-acyl carrier protein synthase III (FabH) inhibitors, *Eur. J. Med. Chem.* 57 (2012) 373-382. (c) Y. Zhou, Q.-R. Du, J. Sun, J.-R. Li, F. Fang, D.-D. Li, Y. Qian, H.-B. Gong, J. Zhao, H.-L. Zhu, Novel Schiff-Base-Derived FabH Inhibitors with Dioxygenated Rings as Antibiotic Agents, *ChemMedChem* 8 (2013) 433-441.
- [24] D. Seeliger, B.L. de Groot, Ligand docking and binding site analysis with PyMOL and Autodock/Vina, *J. Comput. Aided Mol. Des.* 24 (2010) 417-422.
- [25] X. Qiu, C.A. Janson, W.W. Smith, M. Head, J. Lonsdale, A.K. Konstantinidis, Refined structures of beta-ketoacyl carrier protein synthase III, *J. Mol. Biol.* 307 (2001) 341-356.
- [26] D.C. McKinney, C.J. Eyermann, R.-F. Gu, J. Hu, S.L. Kazmirski, S.D. Lahiri, A.R. McKenzie, A.B. Shapiro, G. Breault, Antibacterial FabH Inhibitors with Mode of Action Validated in *Haemophilus influenzae* by in Vitro Resistance Mutation Mapping, *ACS Infect. Dis.* 2 (2016) 456-464.
- [27] S. Barkallah, M. Boukraa, H. Zantour, B. Baccar, Action des enamines sur les monochlorophosphines: synthese des  $\beta$ -cetophosphonates, *Phosphorus Sulfur Silicon Relat. Elem.* 108 (1996) 51-56.
- [28] A. Palm, H. Werbin, Infrared study of the N-OH group in alpha and beta oximes, *Can. J. Chem.* 32 (2011) 858-863.
- [29] J.K. Gillie, J. Hochlowski, G.A. Arbuckle-Keil, Infrared spectroscopy, *Anal. Chem.* 72 (2000) 71-80.
- [30] Z. Hana, S. Shen, F. Zheng, H. Hu, J. Zhanga S. Zhu, Copper-catalyzed synthesis of oxime ethers from iminoxy radical (CN-O) and maleimides via radical addition, *Tetrahedron Lett.* 60 (2019) 151-188.
- [31] R. Barnes, R. Gore, R. Stafford, V. Williams, Organic analysis and infrared spectrometry, *Anal. Chem.* 20 (1948) 402-410.

- [32] J.R. Durig, J.S. Diyorio, Vibrational spectra and structure of organophosphorus compounds: VII. IR and Raman spectra of  $(\text{CH}_3\text{O})_3\text{P}=\text{S}$ , *J. Mol. Struct.* 3 (1969) 179-190.
- [33] I.H. Boyaci, H.T. Temiz, H.E. Geniş, E.A. Soykut, N.N. Yazgan, B. Güven, R.S. Uysal, A.G. Bozkurt, K. İlaslan, O. Toruna, F.C.D. Şeker, Dispersive and FT-Raman Spectroscopic Methods in Food Analysis, *RSC Adv.* 5 (2015) 56606-56624.
- [34] H.W. Thompson, The correlation of vibrational absorption spectra with molecular structure, *J. Chem. Soc.* (1948) 328-331.
- [35] (a) G.C. Levy, G.L. Nelson, Carbon-13 NMR study of aliphatic amides and oximes. Spin-lattice relaxation times and fast internal motions, *J. Am. Chem. Soc.* 94 (1972) 4897- 4901. (b) N. Naulet, H.L. Filleux, G.J. Martin, J. Pornet, Etude par RMN du carbone des systèmes C=N: imines, phénylhydrazones, semicarbazones, amidines, iminoéthers, *Org. Magn. Resonance.* 7 (1975) 326-330. (c) H. Slimani, S. Touil, New Routes to  $\beta$ -Iminophosphonates, Phosphineoxides, and Sulfides, *Phosphorus, Sulfur Silicon Relat. Elem.* 186 (2011) 1655-1664. (d) A. Wahbi, S. Touil, Synthesis of New Phosphonoamide and Phosphonocaprolactam Derivatives via the Diethyl Chlorophosphate-Promoted Beckmann Rearrangement of  $\gamma$ -Phosphonyloximes, *Heter. Chem.* 26 (2015) 397-404.
- [36] H.-K. Fun, S. Chantrapromma, S. Rai, P. Shetty, A.M. Isloor, 2-[(4-tert-Butylanilino)(phenyl)methyl]cyclohexanone, *Acta Crystallogr. E*65 (2009) 539-540.
- [37] D. Cremer, J. A. Pople, General definition of ring puckering coordinat, *J. Am. Chem. Soc.* 97 (1975) 1354-1358.
- [38] L. Peng, C. Liu, N. Li, W. Zhong, L. Mao, S.-R. Kirk, D. Yin, Direct cyclohexanone oxime synthesis via oxidation–oximization of cyclohexane with ammonium acetate, *Chem. Commun.* 56 (2020) 1436-1439.
- [39] (a) P.R. Olivato, D.S. Ribeiro, J. Zukerman-Schpector, G. Bombieri, Self-association and stereochemistry study of 2-methylthio-, 2-dimethylaminocyclohexanone oximes and the parent cyclohexanone oxime, *Acta Cryst.* B57 (2001) 705-713. (b) S.D. Yeoh, B.L. Harris, T.J. Simons, J.M. White, Structure correlation study of the beckmann rearrangement: X-ray structural analysis and  $^{13}\text{C}$ – $^{13}\text{C}$  1-bond coupling constant study of a range of cyclohexanone oxime derivatives, *Aust. J. Chem.* 65 (2012) 905-917.
- [40] C.-C.Tsaia, C.-Y. Zhong, I. Wang, S.-B. Liu, W.-H. Chen, T.-C. Tsai, Vapor phase Beckmann rearrangement of cyclohexanone oxime over MCM-22, *App. Catal. A: General*, 267 (2004) 87-94.

- [41] M. Anilkumar, W.F. Hölderich, Highly active and selective Nb modified MCM-41 catalysts for Beckmann rearrangement of cyclohexanone oxime to  $\epsilon$ -caprolactam, *J. Catal.* **260** (2008) 17-29.
- [42] D. Cremer, General definition of ring puckering coordinates, *J. Am. Chem. Soc.* **97** (1975) 1354-1358.
- [43] (a) R. Galeazzi, C. Marucchini, M. Orenaa, C. Zadrab, Molecular Structure and Stereoelectronic Properties of Herbicide Sulphonylureas, *Bioorg. Med. Chem.* **10** (2002) 1019-1024. (b) R. Galeazzi, C. Marucchini, M. Orena, C. Zadra, Stereoelectronic properties and activity of some imidazolinone herbicides: A computational approach. *J Mol Struct-Theochem.* **640** (2003) 191-200. (c) L. Padmaja, C. Ravikumar, D. Sajan, I. Hubert Joe, V.S. Jayakumar, Density functional study on the structural conformations and intramolecular charge transfer from the vibrational spectra of the anticancer drug combretastatin-A2. *J Raman Spectrosc.* **40** (2009) 419-28. (d) R. Swisłocka, E. Regulska, J. Karpinska, G. Swiderski, W. Lewandowski, Molecular Structure and Antioxidant Properties of Alkali Metal Salts of Rosmarinic Acid. Experimental and DFT Studies, *Molecules.* **24** (2019) 2645.
- [44] (a) D.Y. Curtin, E.J. Grubbs, C.G. McCarty, Uncatalyzed syn-anti Isomerization of Imines, Oxime Ethers, and Haloimines, *J. Am. Chem. Soc.* **88** (1966) 2775-2786. (b) H. Kessler, Thermal isomerization about double bonds: Rotation and inversion, *Tetrahedron.* **30** (1974) 1861-1870. (c) R.D. Bach, G.J. Wolber, Theoretical study of the barrier to nitrogen inversion in N-cyano- and N-diazoformimine. Mechanism of the Schmidt reaction, *J. Org. Chem.* **47** (1982) 239-245. (d) P. Garrat, S. Thom, R. Wrigglesworth, Stereoisomerism in N-cyano-O-phenylisoureas and related compounds, *Tetrahedron.* **50** (1994) 12211-12218. (e) T. Asano, H. Furuta, H.-J. Hofmann, R. Cimiraglia, Y. Tsuno, M. Fujio, Mechanism of thermal Z/E isomerization of substituted N-benzylideneanilines. Nature of the activated complex with an sp-hybridized nitrogen atom, *J. Org. Chem.* **58** (1993) 4418-4423. (f) M. Raban, E. Carlson, Syn-anti isomerism in an N-benzenesulfonylimine. Mechanism of stereomutation at the carbon-nitrogen double bond, *J. Am. Chem. Soc.* **93** (1971) 685-691. (g) G.E. Hall, W.J. Middleton, J.D. Roberts, Nuclear Magnetic Resonance Spectroscopy. Kinetics of Isomerization of Para-Substituted Hexafluoroacetone N-Phenylimines, *J. Am. Chem. Soc.* **93** (1971) 4778-4781. (h) H.-J. Hofmann, T. Asano, R. Cimiraglia, On the conformation of the inversion state in the thermal E,Z isomerization of aromatic azomethines, *J. Chem. Soc., Chem. Commun.* (1991) 295-



296. (i) N.P. Marullo, E.H. Wagener, Isomerization Rates of Iminocarbonates, *J. Am. Chem. Soc.* 88 (1966) 5034-5035. (j) F. Kerek, G. Ostrogovich, Z. Simon, Mechanism of the uncatalysed syn–anti-isomerization of imine systems. Part IV. A theoretical study of the influence of substituents, *J. Chem. Soc. B.* (1971) 541-544. (k) J. Galvez, A. Guirado, A theoretical study of topomerization of imine systems: Inversion, rotation or mixed mechanisms?, *J. Comput. Chem.* 31 (2010) 520-531.
- [45] (a) Y. Arfaoui, M.-L. Efrat, N. Besbes, Theoretical investigations of the mechanistic pathway of the thermal rearrangement of substituted N-acyl-2,2-dimethyl aziridines, *J. Mol. Model.* 19 (2013) 4603-4612. (b) M. Chebbi, Y. Arfaoui, Reactivity of pyrazole derivatives with halomethanes: A DFT theoretical study, *J. Mol. Model.* 24 (2018) 198-208.
- [46] J.T. Tsay, W. Oh, T.J. Larson, S. Jackowski, C.O. Rock, Isolation and Characterization of the Beta-ketoacyl-acyl Carrier Protein Synthase III Gene (fabH) from Escherichia Coli K-12, *J. Biol. Chem.* 267 (1992) 6807-6814.
- [47] Y. Luo, L.R. Zhang, Y. Hu, S. Zhang, J. Fu, X.M. Wang, H.L. Zhu, Synthesis and Antimicrobial Activities of Oximes Derived from *O*-Benzylhydroxylamine as FabH Inhibitors, *ChemMedChem* 7 (2012) 1587-1593.
- [48] R.A. Laskowski, M.B. Swindells, LigPlot+: multiple ligand-protein interaction diagrams for drug discovery, *J. Chem. Inf. Model.* 51 (2011) 2778-2786.